How to cite: *Angew. Chem. Int. Ed.* **2024**, *63*, e202402885
doi.org/10.1002/anie.202402885

Organometallic Chemistry

Visible-Light Activation of Diorganyl Bis(pyridylimino) Isoindolide Aluminum(III) Complexes and Their Organometallic Radical Reactivity

Jonas O. Wenzel, Johannes Werner, Alexander Allgaier, Joris van Slageren, Israel Fernández, Andreas-Neil Unterreiner, and Frank Breher**

Abstract: We report on the synthesis and characterization of a series of (mostly) air-stable diorganyl bis(pyridylimino) isoindolide (BPI) aluminum complexes and their chemistry upon visible-light excitation. The redox non-innocent BPI pincer ligand allows for efficient charge transfer homolytic processes of the title compounds. This makes them a universal platform for the generation of carbon-centered radicals. The photo-induced homolytic cleavage of the Al–C bonds was investigated by means of stationary and transient UV/Vis spectroscopy, spin trapping experiments, as well as EPR and NMR spectroscopy. The experimental findings were supported by quantum chemical calculations. Reactivity studies enabled the utilization of the aluminum complexes as reactants in tin-free Giese-type reactions and carbonyl alkylations under ambient conditions, which both indicated radical-polar crossover behavior. A deeper understanding of the physical fundamentals and photochemical process was provided, furnishing in turn a new strategy to control the reactivity of bench-stable aluminum organometallics.

[*] J. O. Wenzel, Prof. Dr. F. Breher
Karlsruhe Institute of Technology (KIT)
Institute of Inorganic Chemistry (AOC)
Engesserstraße 15, 76131 Karlsruhe (Germany)
E-mail: breher@kit.edu
Homepage: https://www.aoc.kit.edu/breher/

J. Werner, Prof. Dr. A.-N. Unterreiner
Karlsruhe Institute of Technology (KIT)
Institute of Physical Chemistry (IPC)
Fritz-Haber-Weg 2, 76131 Karlsruhe (Germany)
E-mail: andreas.unterreiner@kit.edu

A. Allgaier, Prof. Dr. J. van Slageren
University of Stuttgart
Institute of Physical Chemistry
Pfaffenwaldring 55, 70569 Stuttgart (Germany)

Prof. Dr. I. Fernández
Universidad Complutense de Madrid
Facultad de Ciencias Químicas, 28040 Madrid (Spain)

Introduction

Aluminum, of which 69 megatons are mined annually,[1] is the third most common element (8 %) and therefore the most abundant metal in the earth's crust.[2] This makes aluminum the preferred choice when metal-induced reactivity is demanded. Substituting transition metals by aluminum in various applications is highly desirable and addresses the principles of Green Chemistry.[3] Unfortunately, many reactivity modes known from d-block chemistry are not accessible for aluminum due to its non-precious character. Consequently, a recent goal of synthetic chemists is to mimic transition metal-like reactivity with aluminum, taking a glance at future applications in catalysis.[4,5] While Lewis acid catalysis with aluminum is a historical field of chemistry,[6] redox-mediated catalyses are scarce due to the energetic gradient between sub- and high-valent oxidation states.[7] The vivid field of Main Group redox chemistry in general,[7,8] and subvalent aluminum chemistry in particular, clearly reflects the interest in approaching aluminum redox cycles in the future.[9,10–13] This is likewise illustrated by modern photo-[14] or electrochemical approaches.[15]

One hotly debated reaction type in transition metal chemistry is the homolytic generation of radicals by ligand-to-metal (LMCT) or ligand-to-ligand charge transfer (LLCT),[16] to achieve, for instance, C–H activation reactions or radical-polar crossover reactivity (Scheme 1a).[17] CT homolysis represents also a promising reaction type for p-block compounds, especially for heavy representatives like tin[18] or bismuth.[19] For compounds of lighter elements, such photoreductive processes usually require harsh UV irradiation due to energetically high-lying acceptor orbitals and high energetics of subvalent metal species.[20] This can be overcome by the coordination of redox non-innocent-ligands (NILs),[4,21] introducing low-lying acceptor orbitals, thus providing access to LLCT processes. Well-known are homolyses of element-carbon bonds within porphyrinoid complexes, especially of Group 14 elements,[22] or NIL-containing boron compounds,[23] like the recent dipyrromethene complexes described by Page and co-workers (Scheme 1b).[24]

Bond homolyses of organoaluminum reagents (AlR_3) require the use of UV irradiation yielding mostly complex mixtures of hydrocarbons and aluminum metal.[25] Kaim showed thermally or light-induced radical formation from highly sensitive Lewis-acid/base adducts of aluminum orga-

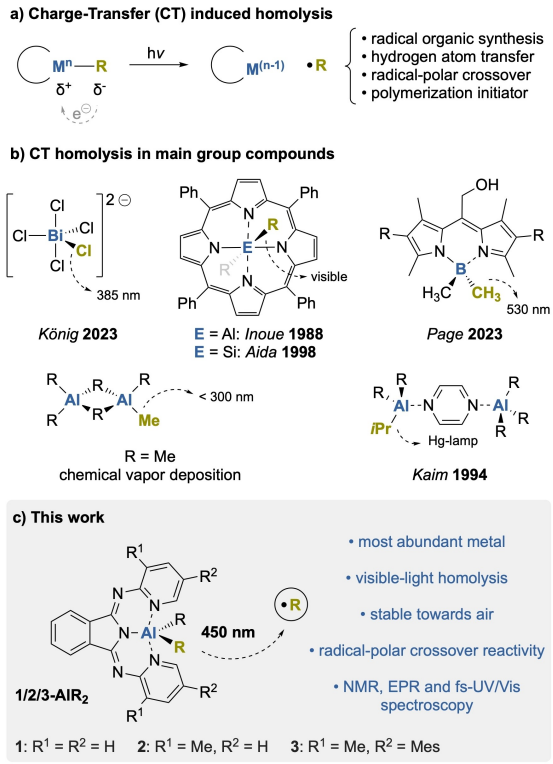

Scheme 1. a) Schematic representation of charge transfer (CT) induced homolysis of M–R bonds especially found in transition metal chemistry. b) Examples for CT homolyses in main group complexes. c) Schematic overview of the targeted CT homolysis in this work.

nometallics and NILs like pyrazine or bipyridine.[26] Also with some redox-active pincer ligands such as bis(imino) pyridine (BIP), the highly nucleophilic AlR_3 compounds already react thermally.[27,28] Instead, aluminum porphyrins represent stable precursors which show photoreactivity upon irradiation, opening up applications as photoinitiators.[29,30] Still, reports of controlled photoreductions in aluminum complexes are scarce, and therefore we were interested in the parameters necessary for CT homolytic processes. We were seeking for a photoactive system, which is highly stable, yet retaining as much as possible of the aluminum organometallic character to enable a broad investigation by multiple methods. Pincer ligands allow more structural variability on the metal atom than porphyrinoids while still benefiting from the chelate effect and potential for redox-activity.[31] We became interested in the tridentate, monoanionic bis(pyridylimino) isoindolide (BPI) ligand, which mimics porphyrinoids in terms of donating atoms and redox-activity.[32] Transition metal complexes of BPI ligands were already applied in asymmetric homogeneous catalysis[33] or artificial photosynthesis,[34] and our group recently investigated the π accepting properties of BPI ligands.[35] Two BPI aluminum complexes were reported by Reddy[36] and Bender,[37] but they were not investigated in view of synthetic photochemistry.

We herein report on the synthesis, characterization, and visible-light chemistry of novel BPI aluminum complexes as well as detailed insights into the physical fundamentals of radical formation in aluminum complexes and their nature of reactivity (Scheme 1c).

Results and Discussion

UV/Vis Spectroscopy

We started our investigation by reproducing the synthesis of **1-AlMe$_2$** reported by Reddy from bis(pyridylimino) isoindoline (**1-H**) and $AlMe_3$ and applied this strategy also for the better soluble ligand systems **2-H** (two additional methyl groups) and **3-H** (two additional methyl and mesityl groups, Scheme 1c). BPI compounds mostly show an intense yellow color, which predominantly arises from π–π* transitions in the UV region up to ~400 nm.[38] Interestingly, **1-AlMe$_2$** shows a red-shifted absorption spectrum (Figure 1) due to the electron-withdrawing effect of the Lewis-acidic aluminum fragment and severe contribution of the nucleophilic Al–C bonds to energetically low-lying transitions by hyperconjugation with the ligands π-system. For the substituted ligands **2** and **3** (Scheme 1), the same trends were observed, but in general, the increasing substitution of the ligand leads to further red shifting of all absorptions (see Section 7 of the Supporting Information).

The UV/Vis spectrum of **1-AlMe$_2$**, calculated by time-dependent density functional theory (TD-DFT) methods using the range-separated hybrid functional cam-B3LYP, nicely reproduces the experimental spectrum (Figure 2a). The first electronic excitation (452 nm) shows strong charge transfer (CT) contribution, which reorganizes electron density from Al–C bonds into π* orbitals of BPI, as visualized in the difference density plot (Figure 2b). According to computations, this ligand-to-ligand charge transfer (LLCT) contributes also to some of the higher energetic absorptions, but the first absorption at ~22,500 cm^{-1} shows the largest charge transfer character. A comparison of experimental and calculated spectra illustrates that, alongside purely electronic transitions, a pronounced vibrational progression is present in **1-AlMe$_2$** with wavenumbers

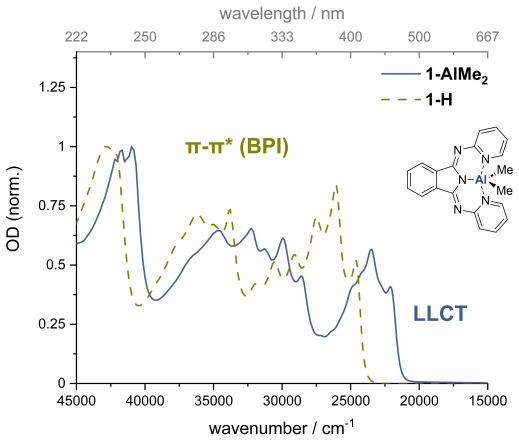

Figure 1. UV/Vis spectra of **1-H** and **1-AlMe$_2$** in *n*-hexane (1 mmol/L) showing normalized optical densities (OD).

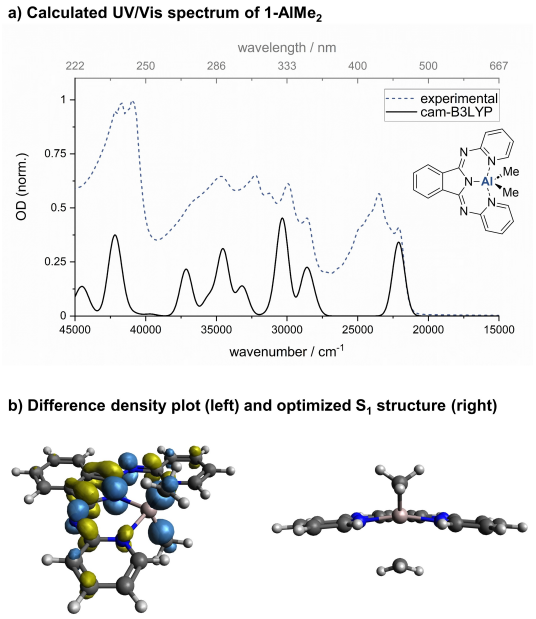

Figure 2. a) Experimental UV/Vis spectrum of **1-AlMe$_2$** (blue dotted) and the spectrum computed on the cam-B3LYP/def2-TZVPD/D4 level of theory (black, applied gaussian linewidth of 1000 cm^{-1}, absolute energy corrected by 5850 cm^{-1} (0.73 eV) with respect to the experiment). b) Left: Obtained difference density plot of first excitation of **1-AlMe$_2$** (blue: decreasing; yellow: increasing; isovalue 0.003). Right: Side-view on S_1^{min} structure of **1-AlMe$_2$** optimized on the cam-B3LYP/def2-TZVPD/D4 level of theory.

between 1400 cm^{-1} and 1500 cm^{-1}. In line with the literature and performed DFT calculations, these frequencies are characteristic of the BPI skeletal vibrations.[39] A possible optimized structure in the gas phase of the first electronic excited state of **1-AlMe$_2$** was located at the TD-DFT level (Figure 2b). Interestingly, one of the two Al–C bonds is already strongly elongated from 1.994 Å in the ground state to 2.429 Å in the S_1 state. This suggests a feasible and almost barrierless homolytic Al–C bond cleavage from the S_1 state. Furthermore, the former double bonds in the BPI ligand of **1-AlMe$_2$** are systematically elongated by ~30 pm upon electronic excitation, while former single bonds are likewise shortened. Such bond length alterations were shown to be the consequence of the increased electron density in the ligand scaffold as the antibonding π* orbitals get populated.[35]

Initial Photoreactivity

Irradiation of **1-AlMe$_2$** in C_6D_6 with 450 nm LEDs (500 mW) indeed led to an intense dark color of the solution. The absorption band around 450 nm, which witnesses the presence of hyperconjugated Al–C bonds, decreased within several seconds (Figure 3). In benzene, increasing absorbance at around 350 nm and an isosbestic point at 377 nm indicated the formation of photoproducts that seemed likewise to be photodegraded over time albeit much slower (gray dotted line in Figure 3). ^{1}H NMR

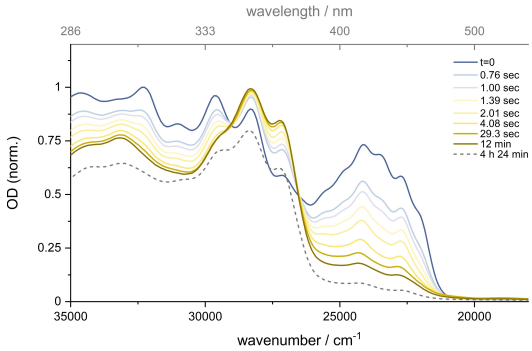

Figure 3. Series of stationary UV/Vis spectra of **1-AlMe$_2$** in C_6H_6 after different times of irradiation with a 450 nm LED (500 mW).

spectroscopic investigations revealed the complete vanishing of the starting material and an unidentified mixture of various photoproducts. We note in passing that the dark color was likewise observed when solutions were stored under ambient sunlight, but the darkening was much slower due to the low intensity of ambient light compared to LEDs.

When the irradiated mixtures of **1-AlMe$_2$** were exposed to ambient air, the dark color vanished and turned back to yellow indicating the formation of highly air-sensitive compounds during the photoreaction. Refluxing **1-AlMe$_2$** in toluene overnight confirmed both its thermal stability and the photochemical nature of the described phenomena. When the photoreaction was repeated in the presence of TEMPO, the formation of Me-TEMPO and one new BPI species, putatively **1-Al(tempo)$_2$**, was observed (Scheme 2). Spin trapping with 5,5-dimethyl-pyrroline *N*-oxide (DMPO) and the sterically more demanding **3-AlMe$_2$** gave the corresponding Me-substituted nitroxide radical of DMPO as detected by cw-EPR spectroscopy, which witnesses the occurrence of methyl radicals (Scheme 2).

We suggest that unselective ligand alkylation is the main reaction pathway that usually defines the fate of the formed radicals. Alkylation of non-innocent ligands (NILs) by aluminum organometallics is often already proceeding without the need for light.[27,28,40] In our case, however, the combination of the electron-rich Al–C bond with the π-accepting properties of the BPI ligand seems to draw a fine line between avoided thermal and accessible photo-activated reactivity. Incidentally, we found that irradiation of **2-AlMe$_2$** for ten minutes as suspension in dimethyl sulfoxide (DMSO) leads predominantly to the methylation of the quaternary carbon atom of the phthaloyl-backbone (Scheme 2). This reaction gave the photoproduct **2^{Me}-AlMe** clean enough to enable characterization from the crude mixture by NMR spectroscopy thus supporting our proposal of ligand alkylation (thermodynamic and kinetic details obtained by DFT can be found in Section 11 of the Supporting Information).

cw-X-Band EPR Spectroscopy

After 1 s irradiation (λ_{exc} = 450 nm) of EPR-silent **1-AlMe$_2$** in toluene solution within the EPR resonator at ambient

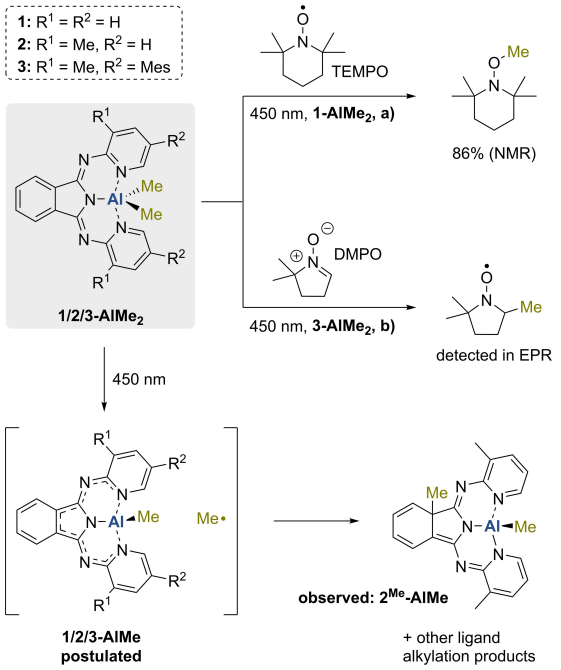

Scheme 2. Radical trapping with tetramethylpiperidine N-oxide (TEMPO) and spin trapping with 5,5-dimethyl-pyrroline N-oxide (DMPO) of the methyl radical formed by homolysis of **1-AlMe$_2$** or **3-AlMe$_2$**. a) 5.00 equiv. TEMPO, C_6D_6, unstirred, 450 nm, r.t., overnight. b) 10.0 equiv. DMPO, C_6D_6, 450 nm, r.t., 4 h.

temperatures under argon, a weak EPR signal was observed. Upon further irradiation, the signal intensity first increased before reaching a stable value. The signal is stable on a timescale of minutes. The spectrum shown in Figure 4 is centered around a g value of 2.0033 and shows a clear splitting into multiple lines, where the central line is more intense than the remaining four.

Such a spectrum is not compatible with a single species scenario. Therefore, we suggest the presence of at least two or more paramagnetic transient species, where the first species gives rise to an unresolved single-line EPR spectrum

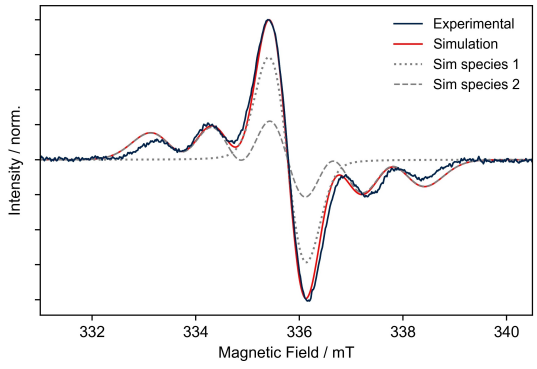

Figure 4. X-band cw-EPR spectra of **1-AlMe$_2$** in toluene (10^{-3} M) recorded after 8 s irradiation (450 nm). g_{iso} = 2.0033, 9.415 GHz, Modulation amplitude 5.00 G, 40 ms conversion time, 5 mW microwave power, 2 scans. The simulation features two species that coexist in the solution.

and the second features hyperfine splitting. We attribute the single-line spectrum to a ligand-based radical without significant contribution of the aluminum atom to the singly occupied molecular orbital (SOMO). This assignment is corroborated by the recently published EPR spectrum of the radical dianion of the methyl-substituted BPI ligand (**2-K$_2$**)[35] featuring only small hyperfine couplings, which would not be resolved on account of the line width. A possible species is **1-AlMe•** formed as escape product after homolytic Al–Me bond splitting, where the corresponding •CH_3 radical is likely trapped by the used solvent or another BPI species. This is supported by theoretical calculations at the PBE0/IGLO-III level on **1-AlMe•** (Table S9, Figure S179) that show delocalized spin density on the BPI ligand leading to small hyperfine coupling constants (~2 MHz) and very little spin density on the aluminum atom. Using the calculated *hfc* and minimal Lorentzian broadening, the single central line in the experimental spectrum is perfectly reproduced (Figure 4, Sim species 1).

The second species possesses much larger hyperfine splittings, which different scenarios could account for. One would be a species with substantial spin density on the aluminum atom (I = 5/2, 100 % natural abundance), giving rise to a 1:1:1:1:1:1 sextet. In that case, the *hfc* of 27.8 MHz extracted from simulations seems reasonable for a ligand-centered radical with some spin density on aluminum like in carbene-stabilized aluminum radicals.[10] A large spin density on aluminum would give much larger *hfc* as it was reported for $[AlH_3]^{\bullet-}$ with high σ character (A = 432 MHz),[41] or reduced dialanes as examples with high π character of the SOMO (A = 174 MHz).[11,13] Alternatively, a quintet spectrum could be due to coupling of the electron spin to two equivalent I = 1 ^{14}N nuclear spins, leading to a quintet with 1:2:3:2:1 intensity ratios. Such a species could be the result of a more localized spin density on the coordinating nitrogen atoms in the BPI ligand. The relatively strong *hfc* (A = 31 MHz) may be due to substantial σ character of the SOMO in the transient species and falls within the range reported for aluminum compounds in literature.[42] We could not reproduce the coupling strength by calculations, because the exact structure of the photoproduct is unknown, making simulation challenging as recently discussed for aluminum radicals.[12] The simulation shown in Figure 4 (red line) is the best obtained fit and consists of the computed species **1-AlMe•** and a species with two couplings to nitrogen (Figure 4, Sim species 2, for details see Section 8 of Supporting Information). Our findings support the occurrence of single-electron processes and BPI radicals as transient species.

Transient UV/Vis Spectroscopy

We further investigated **1-AlMe$_2$** as well as the ligand **1-H** as reference system by transient UV/Vis laser spectroscopy on the femtosecond (fs) to nanosecond (ns) time scale to gain more insight into the elementary steps of the Al–C bond cleavage. Accordingly, **1-AlMe$_2$** was excited with 400 nm (see Figure S123) and 340 nm fs laser pulses. Both transient

spectra are characterized by a rise of a broad absorption band with a positive value of the pump-induced optical density difference ($\triangle mOD$) as exemplarily shown in Figure 5. This band extends from about 450 to 580 nm with a tail towards longer wavelengths and emerged within about 500 fs. The cut-off below 450 nm is due to a pronounced ground state absorption of **1-AlMe$_2$**. As a result, no light reached the detector and therefore no ground-state-bleaching was observable.

The broad absorption in the transient spectrum is due to excited state absorption (ESA). In principle, an additional small contribution to this ESA band may arise from stimulated emission (SE), which would manifest itself as a negative contribution to the ESA band. The contribution of SE is only indirectly observable in the transient traces, but clearly visible in stationary fluorescence spectra (Figure S121). The overall weak SE is consistent with the very low fluorescence quantum yield of **1-AlMe$_2$** ($\Phi = 3.9 \cdot 10^{-4}$). In the transient spectra, the ESA rises within the time resolution of the title experiment (100 fs) indicating ultrafast vibrational motion in the excited state. A possible explanation is the vertical excitation of **1-AlMe$_2$** into a vibrationally hot singlet excited Franck–Condon state, followed by fast structural reorganization. Such reorganization can occur in the sub-picosecond (ps) regime,[43] opening a pathway to photodegradation, which has been postulated to be unlikely for highly fluorescent complexes with an $AlMe_2$ moiety.[44] Furthermore, this is consistent with the strong vibrational progression observed in stationary UV/Vis spectroscopy and the structurally distorted S_1^{min} geometry found by TD-DFT computations (vide supra). The fact that the transient absorption spectra obtained by excitation with 340 nm ($S_2 \leftarrow S_0$) and 400 nm ($S_1 \leftarrow S_0$) laser pulses are nearly identical indicates ultrafast internal conversion between excited singlet states, faster than the time resolution of our setup. This is followed by the discussed structural relaxation to the S_1^{min} state. The ligand **1-H** also showed the fast development of an ESA band superimposed by a weak SE band within several hundred fs but its intensity decreased almost completely within 50 ps (Figure S122). The fluorescence quantum yield for **1-H** is also low ($\Phi = 6.7 \cdot 10^{-6}$), thus suggesting an ultrafast internal conversion likely through a conical intersection as main decay channel. **1-AlMe$_2$** instead, showed a much slower ground state recovery, as evidenced by the persistence of the absorption even after ~1 ns (Figure 5).

To obtain more information about the underlying channels of the decaying ESA band, a global analysis of the main feature between 450 and 580 nm was performed (see Section 5 of the Supporting Information). Three time constants are necessary for an adequate fit. This suggests at least three different processes by which the S_1^{min} state is depopulated. The first time constant τ_1 was in the order of 1 ps. It was assumed to belong to non-radiative $S_0 \leftarrow S_1$ internal conversion since an equally fast process was observed for photostable **1-H** (Figure S122). The time constants τ_2 and τ_3 were determined to be around 30 ps and greater than 100 ps, respectively, and do not have an equivalent counterpart in **1-H** indicating excited state channel branching. We hypothesize that at least one of these two time constants is part of the photoactive channel. Also, intersystem crossing (ISC) to the triplet surface—as theoretically predicted for the free isoindoline[45] and various hydroxyquinolinato[46] or phthalocyanine aluminum complexes[47]—should be taken into account. We further processed the spectra by applying global fits and calculated the decay-associated difference spectra as well as wavelength-dependent relative amplitude ratios to estimate the relative probability with which each channel is populated. Accordingly, A_1^{rel} as well as A_3^{rel} varied between 35 % and 45 % and A_2^{rel} between 20 % and 25 % (Table S6, Figure S127).

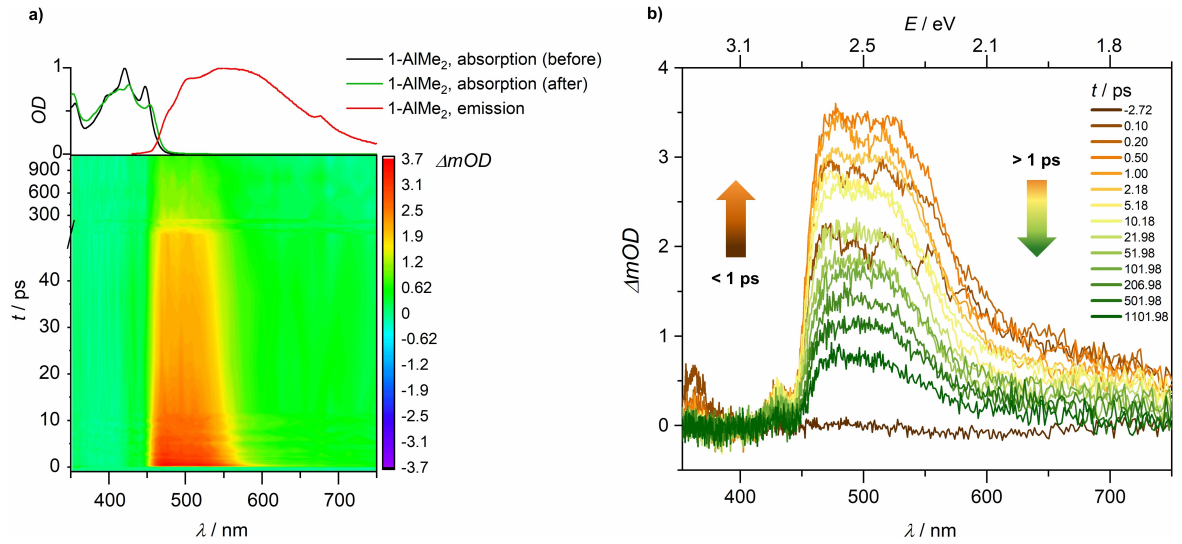

Figure 5. a) Bottom: contour diagram ($\lambda_{ex} = 340$ nm, $E_{ex} = 0.62$ µJ, $OD_{340} = 0.87$), top: stationary absorption (before and after transient measurement) and emission spectrum of **1-AlMe$_2$**. b) Transient absorption spectra of **1-AlMe$_2$** obtained from profiles of the contour diagram at different delay times.

This indicates that the probability of **1-AlMe$_2$** to follow the photoactive channel after excitation to the S_1 state is high (at least 20 %), which is consistent with the extremely fast homolysis observed experimentally. In summary, we conclude that irradiation of **1-AlMe$_2$** with varied wavelengths ends up in the S_1^{min} state from which it can either relax radiationless back into the ground state or undergo photoreaction. Together with all previous findings, this leads us to finally postulate that the poor fluorescence of **1-AlMe$_2$** is the consequence of a very efficient and fast transformation of light into a dissociative vibrational mode, which leads partly to a critical cleavage of the Al–C bond to give the methyl radical and the "masked" Al(II) radical **1-AlMe•**.

Synthesis

After our initial results supported the homolytic LLCT of BPI aluminum complexes, we became interested in the general applicability of the generation of different carbon-centered radicals. The corresponding phenyl-substituted complexes **1-AlPh$_2$**, **2-AlPh$_2$** and **3-AlPh$_2$** were synthesized by deprotonating the free ligands with easily accessible $AlPh_3 \cdot Et_2O$. For the further scope of organic substituents, ligand **2** was mainly used as it usually shows better solubility than **1**, comprises a suitable ^{1}H NMR probe due to the methyl moiety, and still easy synthetic accessibility. The complexes **2-AlEt$_2$**, **2-Al*i*Bu$_2$**, **2-Al*t*Bu$_2$**, **2-AlMeCl**, **2-AlCl$_2$** were synthesized following the same deprotonation strategy by using $AlEt_3$, iBu_2AlH (DIBAL), $AltBu_3$, Me_2AlCl, and $EtAlCl_2$, respectively. Except for $AltBu_3$, all reagents were commercially purchased and used as received making the corresponding aluminum complexes readily accessible in two steps from purchasable starting materials. To also investigate a non-aromatic sp^2-hybridized and a sp-hybridized carbon moiety, **2-Al(CH=CH$_2$)$_2$** and **2-Al(C≡C-TMS)$_2$** were synthesized from **2-AlCl$_2$** by salt metathesis (Figure 6a). All BPI aluminum complexes can be easily purified by recrystallization and mostly boiling toluene is recommended as the solvent of choice. Subsequently, all synthesized complexes were investigated by single-crystal X-ray diffraction (SC-XRD). Paralleling the two reported solid-state structures of **1-AlMe$_2$** and **1-AlCl$_2$** by Reddy,[36] the obtained crystal structures feature trigonal-bipyramidal coordination of the aluminum atoms (Figure 6b). All structures reveal Al–C bond lengths of ~200 pm independent of the type of carbon substituent. **2-Al*t*Bu$_2$** is the only compound that was found to deviate from the mentioned structural characteristics, as one of the pyridine donors does not coordinate to the sterically strongly shielded aluminum atom leading to tetrahedral coordination of the latter.

We ascertained surprising stability in air for most of the complexes. For instance, **2-AlMe$_2$** was stored as solid under ambient air for several months without any degradation. We even observed astonishing stability in solution with only slight decomposition if large amounts of moisture were present as in non-dried THF or acetone. Treating solutions of **1-AlMe$_2$** with one atmosphere of pure oxygen did not

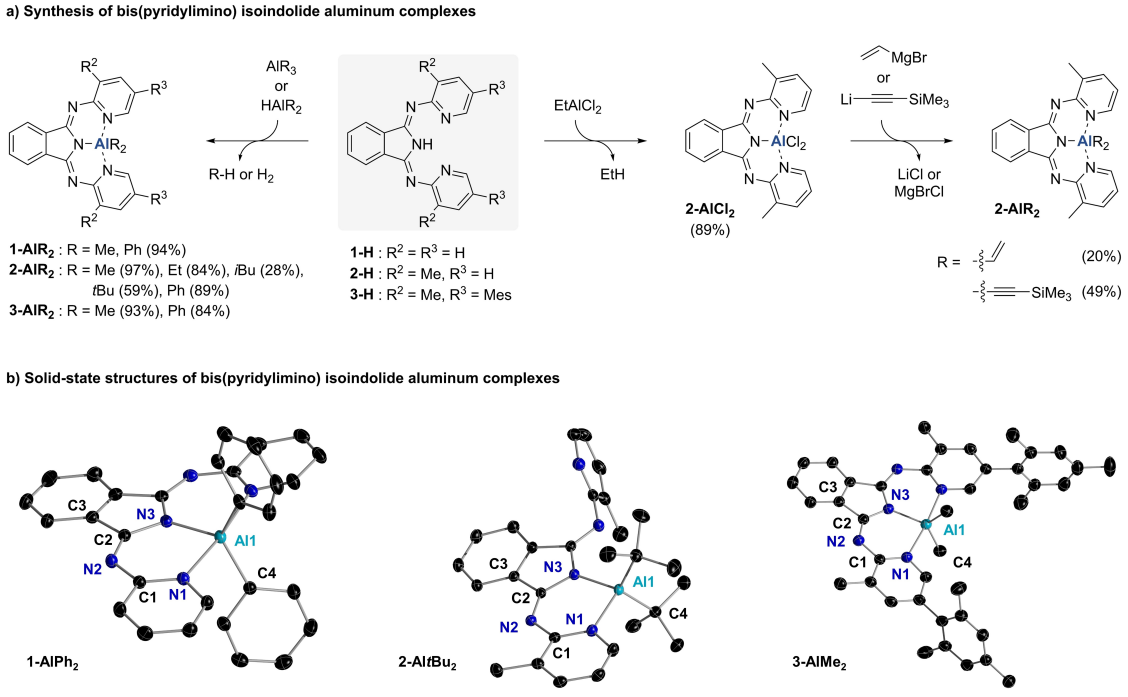

Figure 6. a) Synthesis of varied bis(pyridylimino) isoindolide aluminum complexes. b) Molecular structures of selected BPI aluminum complexes (see also Supporting Information). Hydrogen atoms and crystal lattice solvent molecules were omitted for clarity. Thermal ellipsoids are given at the 30% probability level. Selected bond lengths [pm] and angles [°]: **1-AlPh$_2$**: Al1–N3 191.30(14), Al1–C4 200.00(17), C2–N2 128.8(2); N3–Al1–C4 117.78(7), N3–Al1–N1 87.49(6). **2-Al*t*Bu$_2$**: Al1–N3 190.06(11), Al1–C4 199.74(14), C2–N2 129.76(16); N3–Al1–C4 111.18(6), N3–Al1–N1 91.44(5). **3-AlMe$_2$**: Al1–N3 191.97(18), Al1–C4 198.4(2), C2–N2 130.2(2); N3–Al1–C4 116.18(9), N3–Al1–N1 87.00 (7).

show any reaction. Although experiments with **2-AlMe$_2$** are easily performed under non-Schlenk conditions, we recommend using fresh batches of solvents or molecular sieves to minimize humidity.

Furthermore, the air stability clearly correlates with the hybridization at the carbon atom. While sp^3-hybridized and aromatic derivatives showed only little sensitivity, **2-Al(CH=CH$_2$)$_2$** decomposes in the solid state in air within several days. The sp-hybridized compound **2-Al(C≡C-TMS)$_2$** reacts immediately with air on a time scale of minutes. We therefore conclude that BPI as a palindromic NNN pincer ligand stabilizes the aluminum organometallics by fully saturating their coordination sphere. Therefore, the Lewis-acidity on aluminum is quenched, which appears to diminish hydrolysis rates.

The conversion of **2-AlR$_2$** during irradiation with a 450 nm LED was monitored by ^{1}H NMR spectroscopy (Figure 7). The photolysis of the compounds with sp^3-hybridized substituents seems to follow first-order kinetics with full conversion within a maximum of five minutes (the only exception is **2-Al*t*Bu$_2$**, most likely due to its distinct molecular structure). The sp^2-hybridized vinyl moiety causes a much slower photolysis of the aluminum complex, requiring around 30 minutes for full consumption of the starting material. The phenyl substituent leads to an even slower photolysis, while **2-Al(C≡C-TMS)$_2$** appears to be almost photostable with only 10 % conversion after 16 hours of irradiation. As a result, the tendency of Al–C bond homolysis contrasts the observed trends for air sensitivity concerning the nature of carbon substituent.

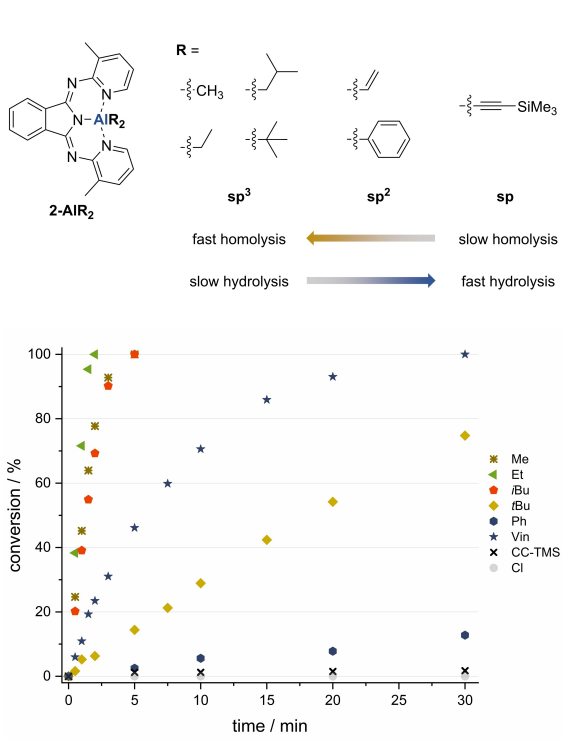

Figure 7. Conversion of **2-AlR$_2$** after different times of irradiation with 450 nm LEDs (500 mW) at ambient temperature within unstirred CD_2Cl_2 solution determined by ^{1}H NMR spectroscopy.

The more polarized bonds of aluminum to, e.g., sp-hybridized carbon scaffolds are expected to show higher bond enthalpies in part due to a larger contribution of Coulomb interaction. This results in a less feasible homolytic bond cleavage but higher reactivity in ionic reactions like hydrolysis. To check this hypothesis, we quantitatively analyzed the bonding situation of model complexes **1-AlR$_2$** having sp^3-methyl, sp^2-vinyl and sp-C≡C-SiH$_3$ substituents with the help of the Energy Decomposition Analysis (EDA) method.[48] The data compiled in Table 1 indicate that the interaction between the radicals [AlR]$^\bullet$ and R$^\bullet$ becomes stronger and stronger when going from sp^3 to sp^2 and to sp substituents, in agreement with the previously discussed trend in Al–C bond homolysis tendency. The trend in the ΔE_{int} term is correlated with the computed Al–C Wiberg Bond Indices (WBIs), which increases from C_{sp3} to C_{sp}. Not surprisingly, the major contribution to the bonding between the [AlR]$^\bullet$ and R$^\bullet$ fragments results from the orbital interaction (i.e. covalent bonding) that displays the same trend. Despite that, we found that the electrostatic attractions, measured by the ΔE_{elstat} term and contributing ca. one third to the total attractive interactions, are enhanced as the substituent is modified from methyl (–83.6 kcal/mol) to alkynyl group (−91.0 kcal/mol). Therefore, our EDA calculations confirm that although the strength of the Al–C bond is comparatively higher in the C_{sp}-substituted systems, the bond becomes also more polarized, showcasing a more significant ionic (i.e. electrostatic) character.

Interestingly, kinetic measurements of **2-AlMe$_2$** homolysis in $CDCl_3$ revealed a rather clean conversion of the compound into **2-AlCl$_2$** with **2-AlMeCl** being the transient species (Figure S22). This implies that the BPI aluminum scaffold initially remains intact after homolysis, and is accessible for follow-up reactions. Furthermore, this corroborates the "masked" Al(II) radical **2-AlMe$^\bullet$** as plausible postulate for the primary homolysis product.

Radical Chemistry

The spin-trapping of the methyl radical, or the formation of **2-AlCl$_2$** by irradiation in chloroform, indicate that both photolysis products are available for subsequent reactions, i.e. as an alternative to the ligand-alkylation pathway (vide

Table 1: EDA values (in kcal/mol)[a] for the Al–C bond in **1-AlR$_2$** systems using [**1-AlR**]$^\bullet$ and R$^\bullet$ as fragments.

	1-AlR$_2$		
	R = CH_3	R = $CH{=}CH_2$	R = $C{\equiv}C{-}SiH_3$
ΔE_{int}	−99.9	−106.7	−145.2
ΔE_{Pauli}	120.8	122.4	131.1
ΔE_{elstat}	−83.6	−86.1	−91.0
ΔE_{orb}	−132.4	−136.7	−180.3
ΔE_{disp}	−4.7	−6.2	−5.0
WBI	0.556	0.57	0.59

[a] All data have been computed at the ZORA-B3LYP-D3/TZ2P//B3LYP-D3/def2-TZVP level.

supra). We probed if some substrates such as electron-deficient alkenes react faster than the BPI scaffold to achieve Giese-type reactions.[49] Therefore, **2-AlMe$_2$** was treated with 1.00 equivalent of acrylonitrile under ambient conditions.

With ambient light, no reaction was detected, but after irradiation with a 450 nm LED for 30 minutes, full conversion of the substrate and 22 % NMR yield of propionitrile were confirmed. We suggested non-efficient hydrogen-atom-transfer (HAT) of the transient cyanopropyl radical to be the reason for the large gap between high conversion and low yield. Thus, we screened several different H atom donor reagents by subjecting 1.00 equivalent of the latter to the photoreactions (Figure 8).

To our surprise, the radical H atom donor Bu_3SnH, the typical reagent for Giese reactions, did show the worst yield, despite full conversion of acrylonitrile. A clear trend is observed that the yield was significantly increased when proton sources were employed, featuring methanol as best additive providing propionitrile in 59–61 % yield. The solvent seems to have little effect on the reaction outcome, but still chlorinated solvents showed the best performance. We noted that higher amounts of added methanol decreased the yield most likely due to partial decomposition of **2-AlMe$_2$**. Besides acrylonitrile, also other alkenes were hydromethylated by **2-AlMe$_2$**/MeOH showing yields between 18–59 % (Scheme 3a). Moreover, the Et, *i*Bu, *t*Bu, vinyl or phenyl radical were successfully transferred in high yields of 72–88 % yield for sp^3-hybridized moieties, and low yields of < 5 % (Ph) and 19 % (vinyl) for sp^2-hybridized substituents (Scheme 3b). These observations corroborate the cyanopropyl-anion as transient species, trapped by the additive rather than the corresponding radical. Still, the attack of the methyl radical to the C=C double bond should be the initial step based on all previous findings. The lower yields in the case of sp^2-carbon radicals support this idea as they typically react less nucleophilic than sp^3-radicals.[50]

Likewise, we observed the formation of half-deuterated biphenyl in 38 % NMR yield when **1-AlPh$_2$** was irradiated in C_6D_6 (Scheme 3d). Therefore, only a radical reaction pathway gives a plausible explanation for the occurrence of this CH-activating aryl-aryl coupling.[51] The primary attacking species is expected to be of radical nature also in the mentioned Giese reactions. A radical-polar crossover behavior, in which the primarily formed cyanopropyl-radical is reduced to the anion by single electron transfer (SET), and subsequently trapped by the proton from MeOH, would be in line with the observations (Scheme 3c). Acceptor-substituted alkyl radicals are typically reduced at potentials around −0.80 V (vs. Fc/Fc$^+$).[52] Although we are not able to comment on the exact redox potential of the relevant BPI aluminum radical, it appears to be a reasonable reductant for this reaction, as we have recently published reduction potentials of around −2.00 V (vs. Fc/Fc*) for the radicals of BPI and its sodium complex.[35] A bonding of the cyanopropyl moiety to the aluminum atom after the redox reaction in a carboalumination-like fashion, similar to the reaction of aluminum porphyrin complexes with acrylates,[29] cannot be excluded. But it is obvious that such a bond would be much more sensitive to hydrolysis than the Al–Me bond because

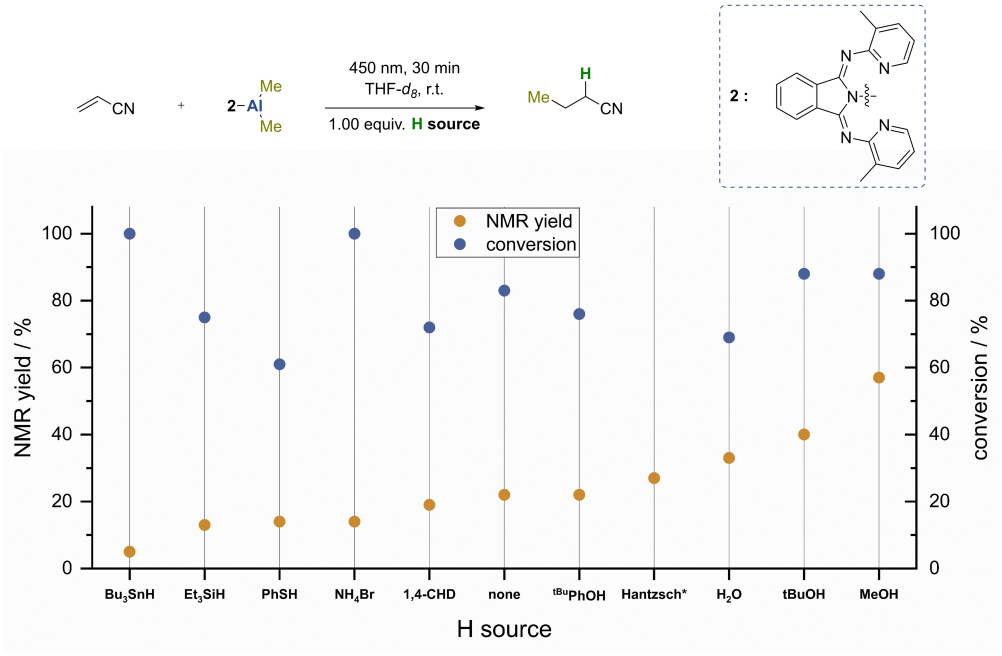

Figure 8. Screening of hydrogen atom sources for the Giese-type hydromethylation of electron-deficient alkenes by **2-AlMe$_2$** under ambient conditions. Yield determined by ^{1}H NMR spectroscopy. Reaction conditions: 0.1 M in THF-d_8, r.t., 450 nm (500 mW), 30 min, 1.00 equiv. of hydrogen atom source, 1.00 equiv. **2-AlMe$_2$**. 1,4-CHD: 1,4-cyclohexadiene. Hantzsch: 1,4-dihydro-2,6-dimethyl-3,5-pyridinedicarboxylic acid diethyl ester. * No conversion is given for the reaction with Hantzsch-ester as signal-overlap in ^{1}H NMR spectra denied accurate determination; it is estimated to < 50 %.

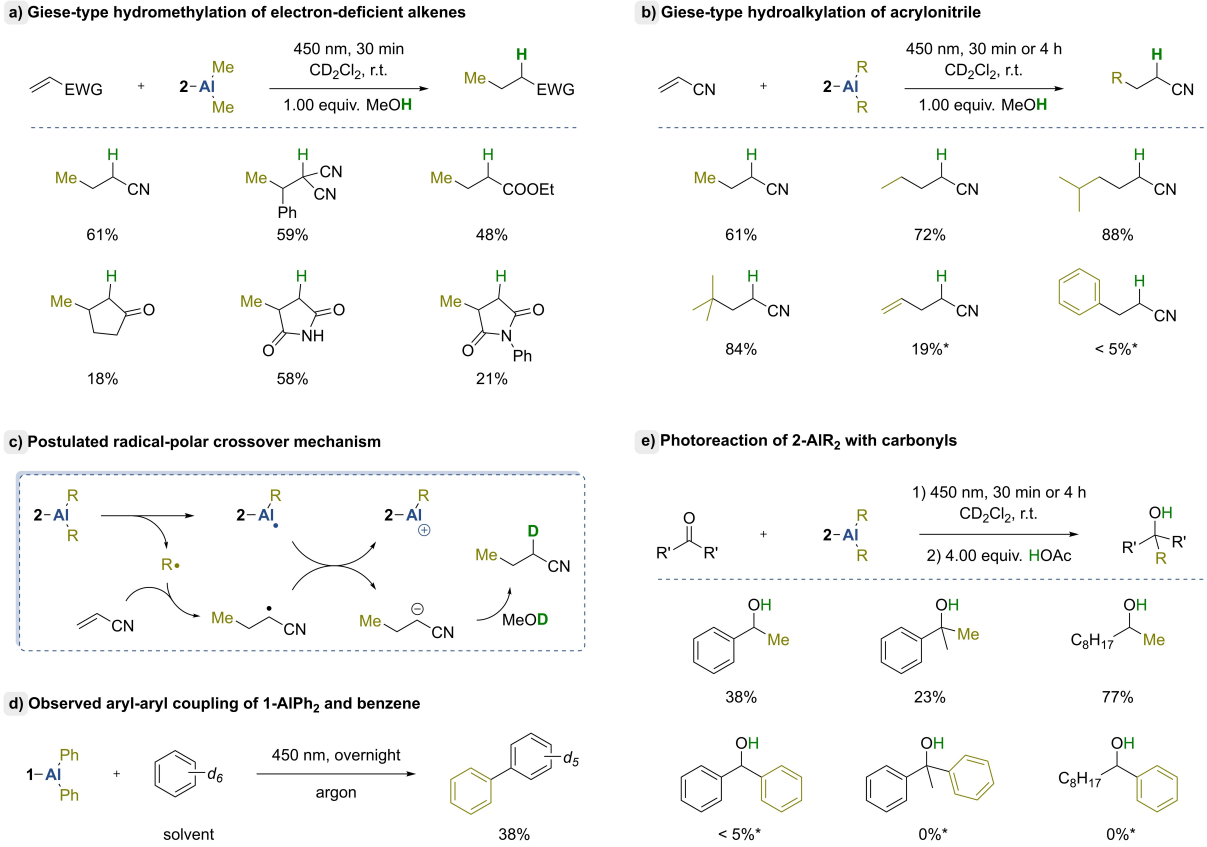

Scheme 3. a) Giese-type hydromethylation of electron-deficient alkenes with 1.00 equiv. **2-AlMe$_2$**. b) Giese-type hydroalkylation of acrylonitrile with 1.00 equiv. **2-AlR$_2$**. c) Postulated radical-polar crossover mechanism of the title Giese-type alkylation. d) Biphenyl formation by reaction of **1-AlPh$_2$** with C_6D_6. e) Alkylation and arylation of C=O bonds by **2-AlR$_2$**. * 4 hours reaction time. All reactions except d) were conducted under ambient air applying a concentration of 0.1 mol/L. Product formation was confirmed by GC-MS and yields were determined by ^{1}H NMR spectroscopy.

of the stabilized carbanionic character (vide supra). Thus, the reaction with MeOH is expected to be fast, forming the experimentally observed propionitrile. MeOH was confirmed as the main source of the proton in the formed propionitrile by deuterium labelling studies using MeOH-d_4. In the case of the present conjugate addition, the change from the radical to the ionic pathway is directly connected to the avoidance of toxic tin reagents. Those toxic reagents typically resemble the largest drawbacks of classical Giese reactions.[53]

To further challenge the proposal of radical-polar crossover reactivity, **2-AlMe$_2$** was treated with benzaldehyde. Radical addition to C=O double bonds is reversible and thermodynamically unfavored.[54] Different studies highlighted that radical alkylation of carbonyls is only possible by preforming hydrogen bonds or by directly following SET processes.[55] First, we noticed almost full conversion of the aldehyde but no product formation when the reaction was conducted under the same conditions as mentioned before. However, when the mixtures were quenched by addition of acetic acid, 1-phenylethanol formation was observed. This leads to the conclusion that the formed methyl radical adds to the aldehyde, which is directly followed by SET from the BPI aluminum radical. A putatively transient aluminum alkoxide probably requires harsher reagents for solvolysis, thus releasing the alkylation product. GC-MS data hinted at the formation of substituted derivatives of benzaldehyde and 1-phenylethanol with additional methyl groups attached to the aromatic ring as side products, clearly indicating radical pathways. Furthermore, the yield for methylation of aliphatic nonanal was higher and the arylation of C=O bonds again proceeded poorly due to the electrophilic nature of phenyl radicals (Scheme 3e).

Conclusion

This work addressed the development of a controlled, visible-light-induced charge-transfer (CT) homolysis of metal-carbon bonds as an important redox-mediated elementary reaction on aluminum organometallics. The coordination of the monoanionic redox-active bis(pyridylimino) isoindolide (BPI) ligand scaffold to AlR_2 fragments gave coordination compounds, which are much more stable towards ambient air than conventional organometallics. As supported by density functional theory calculations, excitation results in the transfer of electron density from the nucleophilic Al–C bond to the π* orbitals of the ligand scaffold, leading to a cleavage of the Al–C bond and the formation of a reduced BPI aluminum radical. This was further supported by spin

and radical trapping experiments as well as EPR spectroscopy and femtosecond UV/Vis spectroscopy. When the homolysis products are not trapped, ligand alkylation is the dominating reaction pathway. We have shown in the form of tin-free Giese-type conjugate additions or C=O alkylations that such formed radicals can alternatively be used synthetically under ambient conditions and that these reactions proceed via radical-polar crossover mechanisms. By applying a variety of methods to gain fundamental information about photochemical processes in Main Group photochemistry, we conclude that the polarity of the metal-carbon bond and the efficiency of energy transfer from light into vibrational modes are the crucial parameters for photoreductive CT homolysis. Further insights into the homolysis mechanism, substitution effects as well as radical chemistry are currently being investigated in our laboratories.

Supporting Information

The authors have cited additional references within the Supporting Information.[56–108] Deposition Number(s) (https://www.ccdc.cam.ac.uk/services/structures?id=doi:10.1002/anie.202402885) 2313487 (for 2-amino-5-mesityl-3-methylpyridine), 2313446 (for **1-AlPh$_2$**), 2313488 (for **2-AlMe$_2$**), 2313489 (for **2-AlEt$_2$**), 2313490 (for **2-Al*i*Bu$_2$**), 2313491 (for **2-Al*t*Bu$_2$**), 2313492 (for **2-AlPh$_2$**), 2313493 (for **2-AlCl$_2$**), 2313485 (for **2-Al(CH=CH$_2$)$_2$**), 2313494 (for **2-Al(C≡C-TMS)$_2$**), 2313495 (for **3-AlMe$_2$**), 2313496 (for **3-AlPh$_2$**) contain(s) the supplementary crystallographic data for this paper. These data are provided free of charge by the joint Cambridge Crystallographic Data Centre and Fachinformationszentrum Karlsruhe http://www.ccdc.cam.ac.uk/structures Access Structures service.

Author Contributions

Jonas Oliver Wenzel: Conceptualization, Investigation (synthesis, quantum chemistry), Validation, Visualization, Writing—Original Draft Preparation. Johannes Werner: Investigation (optical spectroscopy, quantum chemistry), Writing—Review & Editing. Alexander Allgaier: Investigation (EPR-spectroscopy), Writing—Review & Editing. Joris van Slageren: Investigation (EPR-spectroscopy), Writing—Review & Editing. Israel Fernández: Investigation (quantum chemistry). Andreas-Neil Unterreiner: Supervision, Resources, Writing—Review & Editing. Frank Breher: Supervision, Project Administration, Resources, Writing—Review & Editing.

Acknowledgements

This work was financially supported by the *Fonds der Chemischen Industrie* through Kekulé scholarships for J.O.W and J.W. This work was partly carried out with the support of the *Karlsruhe Nano Micro Facility (KNMF)*, a Helmholtz Research Infrastructure at *Karlsruhe Institute of Technology (KIT)* and we thank Prof. Dr. Dieter Fenske, Dr. Olaf Fuhr, Dr. Alexander Hinz, Dr. Felix Krämer, Melina Dilanas and Dr. Christopher Anson for help with SC-XRD. The authors acknowledge support by the state of Baden-Württemberg through bwHPC and the German Research Foundation (DFG) through grants No. INST 40/575-1 FUGG (JUSTUS 2 Cluster), INST 121384/133-1 FUGG (femtosecond laser system) and 358283783 – CRC 1333/2 2022. I. F. is grateful for financial support from the Spanish MCIN/AEI/10.13039/501100011033 (PID2022-139318NB-I00 and RED2022-134287-T). The authors thank Prof. Dr. M. A. R. Meier and Prof. Dr. H. A. Wagenknecht for sharing infrastructure as well as Luis Santos Correa, Mathis Mitha, Christian Pachl and Pascal Rauthe for fruitful discussions. Furthermore, the authors thank Nicole Klaassen for elemental analysis, Helga Berberich for NMR spectroscopic measurements and Lara Hirsch for mass spectrometric measurements. Open Access funding enabled and organized by Projekt DEAL.

Conflict of Interest

The authors declare no conflict of interest.

Data Availability Statement

The data that support the findings of this study are available in the supplementary material of this article.

Keywords: Aluminum · Main Group Chemistry · Non-Innocent Ligands · Organoaluminum Chemistry · Photochemistry

[1] International Aluminium, "Primary Aluminium Production, Annually total for 2022", can be found under https://international-aluminium.org/statistics/primary-aluminium-production/; visited 3rd Oct. 2023.
[2] A. A. Yaroshevsky, *Geochem. Int.* **2006**, *44*, 48.
[3] a) P. T. Anastas, J. C. Warner, *Green Chemistry: Theory and Practice*, Oxford University Press, New York, **1998**; b) P. Anastas, N. Eghbali, *Chem. Soc. Rev.* **2010**, *39*, 301.
[4] P. S. Gahlaut, K. Yadav, D. Gautam, B. Jana, *J. Organomet. Chem.* **2022**, *963*, 122298.
[5] C. Knüpfer, C. Färber, J. Langer, S. Harder, *Angew. Chem. Int. Ed. Engl.* **2023**, *62*, e202219016.
[6] a) C. Ni, X. Ma, Z. Yang, H. W. Roesky, *Eur. J. Inorg. Chem.* **2022**, *2022*; b) G. I. Nikonov, *ACS Catal.* **2017**, *7*, 7257; c) E. Fazekas, P. A. Lowy, M. Abdul Rahman, A. Lykkeberg, Y. Zhou, R. Chambenahalli, J. A. Garden, *Chem. Soc. Rev.* **2022**, *51*, 8793; d) M. E. Z. Velthoen, A. Muñoz-Murillo, A. Bouhmadi, M. Cecius, S. Diefenbach, B. M. Weckhuysen, *Macromolecules* **2018**, *51*, 343.
[7] T. Chu, G. I. Nikonov, *Chem. Rev.* **2018**, *118*, 3608.
[8] a) Z. Feng, S. Tang, Y. Su, X. Wang, *Chem. Soc. Rev.* **2022**, *51*, 5930; b) L. Greb, *Eur. J. Inorg. Chem.* **2022**, *2022*, e202100871; c) H. W. Moon, J. Cornella, *ACS Catal.* **2022**, *12*, 1382; d) J. M. Lipshultz, G. Li, A. T. Radosevich, *J. Am. Chem. Soc.* **2021**, *143*, 1699.
[9] a) X. Zhang, Y. Mei, L. L. Liu, *Chem. Eur. J.* **2022**, *28*, e202202102; b) C. Bakewell, K. Hobson, C. J. Carmalt,

Angew. Chem. Int. Ed. Engl. **2022**, *61*, e202205901; c) J. Hicks, P. Vasko, J. M. Goicoechea, S. Aldridge, *Angew. Chem. Int. Ed. Engl.* **2021**, *60*, 1702; d) K. Hobson, C. J. Carmalt, C. Bakewell, *Chem. Sci.* **2020**, *11*, 6942; e) H. W. Roesky, S. S. Kumar, *Chem. Comm. (Camb)* **2005**, 4027.

[10] B. Li, S. Kundu, A. C. Stückl, H. Zhu, H. Keil, R. Herbst-Irmer, D. Stalke, B. Schwederski, W. Kaim, D. M. Andrada, G. Frenking, H. W. Roesky, *Angew. Chem. Int. Ed. Engl.* **2017**, *56*, 397.

[11] M. Nakamoto, T. Yamasaki, A. Sekiguchi, *J. Am. Chem. Soc.* **2005**, *127*, 6954.

[12] D. Mandal, T. I. Demirer, T. Sergeieva, B. Morgenstern, H. T. A. Wiedemann, C. W. M. Kay, D. M. Andrada, *Angew. Chem. Int. Ed. Engl.* **2023**, *62*, e202217184.

[13] W. Uhl, A. Vester, W. Kaim, J. Poppe, *J. Organomet. Chem.* **1993**, *454*, 9.

[14] a) C. Onneken, T. Morack, J. Soika, O. Sokolova, N. Niemeyer, C. Mück-Lichtenfeld, C. G. Daniliuc, J. Neugebauer, R. Gilmour, *Nature* **2023**, *621*, 753; b) J.-W. Wang, F. Ma, T. Jin, P. He, Z.-M. Luo, S. Kupfer, M. Karnahl, F. Zhao, Z. Xu, T. Lian, Y.-L. Huang, L. Jiang, L.-Z. Fu, G. Ouyang, X.-Y. Yi, *J. Am. Chem. Soc.* **2023**, *145*, 676; c) A. Gualandi, M. Marchini, L. Mengozzi, H. T. Kidanu, A. Franc, P. Ceroni, P. G. Cozzi, *Eur. J. Org. Chem.* **2020**, *2020*, 1486.

[15] T. J. Sherbow, E. J. Thompson, A. Arnold, R. I. Sayler, R. D. Britt, L. A. Berben, *Chem. Eur. J.* **2019**, *25*, 454.

[16] a) F. Juliá, *ChemCatChem* **2022**, *14*; b) R. Zhao, L. Shi, *Org. Chem. Front.* **2018**, *5*, 3018; c) L. H. M. de Groot, A. Ilic, J. Schwarz, K. Wärnmark, *J. Am. Chem. Soc.* **2023**, *145*, 9369; d) J. Liu, L. Lu, D. Wood, S. Lin, *ACS Cent. Sci.* **2020**, *6*, 1317; e) A. Reichle, O. Reiser, *Chem. Sci.* **2023**, *14*, 4449.

[17] a) M. I. Gonzalez, D. Gygi, Y. Qin, Q. Zhu, E. J. Johnson, Y.-S. Chen, D. G. Nocera, *J. Am. Chem. Soc.* **2022**, *144*, 1464; b) B. Maity, S. Dutta, L. Cavallo, *Chem. Soc. Rev.* **2023**, *52*, 5373; c) Z. Zhang, X. Li, D. Zhou, S. Ding, M. Wang, R. Zeng, *J. Am. Chem. Soc.* **2023**, *145*, 7612; d) Á. Velasco-Rubio, P. Martínez-Balart, A. M. Álvarez-Constantino, M. Fañanás-Mastral, *Chem. Comm. (Camb)* **2023**, *59*, 9424; e) J. T. Gavin, R. G. Belli, C. C. Roberts, *J. Am. Chem. Soc.* **2022**, *144*, 21431; f) S. Sharma, J. Singh, A. Sharma, *Adv. Synth. Catal.* **2021**, *363*, 3146; g) L. Capaldo, D. Ravelli, M. Fagnoni, *Chem. Rev.* **2022**, *122*, 1875; h) J.-M. Mörsdorf, J. Ballmann, *J. Am. Chem. Soc.* **2023**, *145*, 23452.

[18] a) J. J. Zuckerman (Ed.) *Advances in Chemistry Series*, *Vol. 157*, American Chemical Society, Washington, DC, **1976**; b) W. Zou, K. L. Mears, J. C. Fettinger, P. P. Power, *Chem. Comm. (Camb)* **2023**, *59*, 13203.

[19] a) D. Birnthaler, R. Narobe, E. Lopez-Berguno, C. Haag, B. König, *ACS Catal.* **2023**, *13*, 1125; b) S. Martinez, C. Lichtenberg, *Synlett* **2023**; c) M. Mato, J. Cornella, *Angew. Chem. Int. Ed. Engl.* **2023**, e202315046.

[20] a) A. Vogler, A. Paukner, H. Kunkely, *Coord. Chem. Rev.* **1990**, *97*, 285; b) A. Vogler, H. Nikol, *Pure Appl. Chem.* **1992**, *64*, 1311.

[21] a) A. Nakada, T. Matsumoto, H.-C. Chang, *Coord. Chem. Rev.* **2022**, *473*, 214804; b) C. M. Lemon, S. J. Hwang, A. G. Maher, D. C. Powers, D. G. Nocera, *Inorg. Chem.* **2018**, *57*, 5333; c) E. I. Carrera, T. M. McCormick, M. J. Kapp, A. J. Lough, D. S. Seferos, *Inorg. Chem.* **2013**, *52*, 13779.

[22] a) J. E. Pia, B. A. Hussein, V. Skrypai, O. Sarycheva, M. J. Adler, *Coord. Chem. Rev.* **2021**, *449*, 214183; b) P. J. Brothers, in *Advances in Organometallic Chemistry*, *v.48* (Eds.: R. West, A. F. Hill), Elsevier textbooks, s.l., **2001**; c) B. Maiti, A. K. Manna, C. McCleese, T. L. Doane, S. Chakrapani, C. Burda, B. D. Dunietz, *J. Phys. Chem. A* **2016**, *120*, 7634; d) J.-Y. Zheng, K. Konishi, T. Aida, *J. Am. Chem. Soc.* **1998**, *120*, 9838.

[23] a) S. Pillitteri, P. Ranjan, E. V. van der Eycken, U. K. Sharma, *Adv. Synth. Catal.* **2022**, *364*, 1643; b) Y. Miyamoto, Y. Sumida, H. Ohmiya, *Org. Lett.* **2021**, *23*, 5865; c) M. Kemmochi, Y. Miyamoto, Y. Sumida, H. Ohmiya, *Asian J. Org. Chem.* **2022**, *11*; d) Y. Sato, Y. Miyamoto, Y. Sumida, T. Hosoya, H. Ohmiya, *Org. Biomol. Chem.* **2020**, *18*, 6598; e) Y. Sato, K. Nakamura, Y. Sumida, D. Hashizume, T. Hosoya, H. Ohmiya, *J. Am. Chem. Soc.* **2020**, *142*, 9938.

[24] K.-Y. Chung, Z. A. Page, *J. Am. Chem. Soc.* **2023**, *145*, 17912.

[25] a) G. S. Higashi, C. G. Fleming, *Appl. Phys. Lett.* **1989**, *55*, 1963; b) J. J. Eisch, J. L. Considine, *J. Am. Chem. Soc.* **1968**, *90*, 6257; c) H. Hoberg, E. Ziegler, *Angew. Chem.* **1967**, *79*, 411; d) J. J. Eisch, J. L. Considine, *J. Organomet. Chem.* **1971**, *26*, C1–C3.

[26] S. Hasenzahl, W. Kaim, T. Stahl, *Inorg. Chim. Acta* **1994**, *225*, 23.

[27] Q. Knijnenburg, J. M. M. Smits, P. H. M. Budzelaar, *Organometallics* **2006**, *25*, 1036.

[28] M. Gallardo-Villagrán, F. Vidal, P. Palma, E. Álvarez, E. Y.-X. Chen, J. Cámpora, A. Rodríguez-Delgado, *Dalton Trans.* **2019**, *48*, 9104.

[29] H. Murayama, S. Inoue, *Chem. Lett.* **1985**, *14*, 1377.

[30] a) Y. Hirai, H. Murayama, T. Aida, S. Inoue, *J. Am. Chem. Soc.* **1988**, *110*, 7387; b) M. Komatsu, T. Aida, S. Inoue, *J. Am. Chem. Soc.* **1991**, *113*, 8492; c) M. Kuroki, T. Watanabe, T. Aida, S. Inoue, *J. Am. Chem. Soc.* **1991**, *113*, 5903; d) T. Aida, S. Inoue, *Acc. Chem. Res.* **1996**, *29*, 39.

[31] G. G. Briand, *Dalton Trans.* **2023**, *52*, 17666.

[32] R. Csonka, G. Speier, J. Kaizer, *RSC Adv.* **2015**, *5*, 18401.

[33] B. K. Langlotz, H. Wadepohl, L. H. Gade, *Angew. Chem. Int. Ed. Engl.* **2008**, *47*, 4670.

[34] S. Saha, S. T. Sahil, M. M. R. Mazumder, A. M. Stephens, B. Cronin, E. C. Duin, J. W. Jurss, B. H. Farnum, *Dalton Trans.* **2021**, *50*, 926.

[35] J. O. Wenzel, I. Fernández, F. Breher, *Eur. J. Inorg. Chem.* **2023**, *26*.

[36] K. Bakthavachalam, N. D. Reddy, *Organometallics* **2013**, *32*, 3174.

[37] J. D. Dang, T. P. Bender, *Inorg. Chem. Commun.* **2013**, *30*, 147.

[38] D. C. Sauer, R. L. Melen, M. Kruck, L. H. Gade, *Eur. J. Inorg. Chem.* **2014**, *2014*, 4715.

[39] a) W. O. Siegl, *J. Org. Chem.* **1977**, *42*, 1872; b) Z. Liu, X. Zhang, Y. Zhang, J. Jiang, *Spectrochim. Acta A Mol. Biomol. Spectrosc.* **2007**, *67*, 1232.

[40] a) Q. Knijnenburg, S. Gambarotta, P. H. M. Budzelaar, *Dalton Trans.* **2006**, 5442; b) L. W. T. Parsons, L. A. Berben, *Chem. Sci.* **2023**, *14*, 8234; c) M.-R. Ke, Z. Chen, J. Shi, Y. Wei, H. Liu, S. Huang, X. Li, B.-Y. Zheng, J.-D. Huang, *Chem. Comm. (Camb)* **2023**, *59*, 9832.

[41] J. R. M. Giles, B. P. Roberts, *J. Chem. Soc. Chem. Commun.* **1981**, 1167.

[42] a) C. T. Farrar, J. T. Leman, S. C. Larsen, J. Braddock-Wilking, D. J. Singel, A. R. Barron, *J. Am. Chem. Soc.* **1995**, *117*, 1746; b) W. Kaim, *J. Am. Chem. Soc.* **1984**, *106*, 1712.

[43] a) M. Iwamura, S. Takeuchi, T. Tahara, *J. Am. Chem. Soc.* **2007**, *129*, 5248; b) N. P. Ernsting, S. A. Kovalenko, T. Senyushkina, J. Saam, V. Farztdinov, *J. Phys. Chem. A* **2001**, *105*, 3443.

[44] F. L. Portwich, Y. Carstensen, A. Dasgupta, S. Kupfer, R. Wyrwa, H. Görls, C. Eggeling, B. Dietzek, S. Gräfe, M. Wächtler, R. Kretschmer, *Angew. Chem. Int. Ed. Engl.* **2022**, *61*, e202117499.

[45] Y. Harabuchi, K. Saita, S. Maeda, *Photochem. Photobiol. Sci.* **2018**, *17*, 315.

[46] R. R. Valiev, V. N. Cherepanov, G. V. Baryshnikov, D. Sundholm, *Phys. Chem. Chem. Phys.* **2018**, *20*, 6121.

[47] T. Nyokong, *Coord. Chem. Rev.* **2007**, *251*, 1707.
[48] a) F. M. Bickelhaupt, E. J. Baerends, in *Reviews in Computational Chemistry* (Eds.: K. B. Lipkowitz, D. B. Boyd), Wiley, **2000**, pp. 1–86; b) M. von Hopffgarten, G. Frenking, *WIREs Comput. Mol. Sci.* **2012**, *2*, 43; c) I. Fernández, in *Applied theoretical organic chemistry* (Ed.: D. J. Tantillo), World Scientific, New Jersey, **2018**, pp. 191–226.
[49] B. Giese, *Angew. Chem. Int. Ed. Engl.* **1983**, *22*, 753.
[50] P. Renaud, M. P. Sibi, *Radicals in Organic Synthesis*, Wiley, Weinheim, **2001**.
[51] A. Wetzel, G. Pratsch, R. Kolb, M. R. Heinrich, *Chem. Eur. J.* **2010**, *16*, 2547.
[52] T. van Leeuwen, L. Buzzetti, L. A. Perego, P. Melchiorre, *Angew. Chem. Int. Ed. Engl.* **2019**, *58*, 4953.
[53] A. L. Gant Kanegusuku, J. L. Roizen, *Angew. Chem. Int. Ed. Engl.* **2021**, *60*, 21116.
[54] M. Salamone, M. Bietti, *Synlett* **2014**, *25*, 1803.
[55] L. Pitzer, F. Sandfort, F. Strieth-Kalthoff, F. Glorius, *J. Am. Chem. Soc.* **2017**, *139*, 13652.
[56] S. Krieck, H. Görls, M. Westerhausen, *Organometallics* **2008**, *27*, 5052.
[57] W. Uhl, *Z. Anorg. Allg. Chem.* **1989**, *570*, 37.
[58] G. R. Fulmer, A. J. M. Miller, N. H. Sherden, H. E. Gottlieb, A. Nudelman, B. M. Stoltz, J. E. Bercaw, K. I. Goldberg, *Organometallics* **2010**, *29*, 2176.
[59] L. van Gerven, J. Talpe, A. van Itterbeek, *Physica* **1967**, *33*, 207.
[60] J. Koziskova, F. Hahn, J. Richter, J. Kožíšek, *Acta Chim. Slov.* **2016**, *9*, 136.
[61] O. V. Dolomanov, L. J. Bourhis, R. J. Gildea, J. A. K. Howard, H. Puschmann, *J. Appl. Crystallogr.* **2009**, *42*, 339.
[62] G. M. Sheldrick, *Acta Crystallogr. Sect. A* **2015**, *71*, 3.
[63] G. M. Sheldrick, *Acta Crystallogr. Sect. C* **2015**, *71*, 3.
[64] C. Schweigert, O. Babii, S. Afonin, T. Schober, J. Leier, N. C. Michenfelder, I. V. Komarov, A. S. Ulrich, A. N. Unterreiner, *ChemPhotoChem* **2019**, *3*, 403.
[65] V. R. Naina, A. K. Singh, P. Rauthe, S. Lebedkin, M. T. Gamer, M. M. Kappes, A.-N. Unterreiner, P. W. Roesky, *Chemistry (Weinheim an der Bergstrasse, Germany)* **2023**, *29*, e202300497.
[66] I. H. M. van Stokkum, D. S. Larsen, R. van Grondelle, *Biochim. Biophys. Acta* **2004**, *1657*, 82.
[67] J. C. Lagarias, J. A. Reeds, M. H. Wright, P. E. Wright, *SIAM J. Optim.* **1998**, *9*, 112.
[68] F. Neese, *WIREs Comput. Mol. Sci.* **2012**, *2*, 73.
[69] F. Neese, F. Wennmohs, U. Becker, C. Riplinger, *J. Chem. Phys.* **2020**, *152*, 224108.
[70] S. Kossmann, F. Neese, *J. Chem. Theory Comput.* **2010**, *6*, 2325.
[71] T. Yanai, D. P. Tew, N. C. Handy, *Chem. Phys. Lett.* **2004**, *393*, 51.
[72] E. Caldeweyher, S. Ehlert, A. Hansen, H. Neugebauer, S. Spicher, C. Bannwarth, S. Grimme, *J. Chem. Phys.* **2019**, *150*, 154122.
[73] C. Adamo, V. Barone, *J. Chem. Phys.* **1999**, *110*, 6158.
[74] F. Weigend, R. Ahlrichs, *Phys. Chem. Chem. Phys.* **2005**, *7*, 3297.
[75] E. Caldeweyher, C. Bannwarth, S. Grimme, *J. Chem. Phys.* **2017**, *147*, 34112.
[76] W. Kutzelnigg, C. Wüllen, U. Fleischer, R. Franke, T. Mourik, in *Nuclear Magnetic Shieldings and Molecular Structure* (Ed.: J. A. Tossell), Springer Netherlands, Dordrecht, **1993**, pp. 141–161.
[77] V. Ásgeirsson, B. O. Birgisson, R. Bjornsson, U. Becker, F. Neese, C. Riplinger, H. Jónsson, *J. Chem. Theory Comput.* **2021**, *17*, 4929.
[78] Gaussian 09, Revision D.01, M. J. Frisch, G. W. Trucks, H. B. Schlegel, G. E. Scuseria, M. A. Robb, J. R. Cheeseman, G. Scalmani, V. Barone, G. A. Petersson, H. Nakatsuji, X. Li, M. Caricato, A. Marenich, J. Bloino, B. G. Janesko, R. Gomperts, B. Mennucci, H. P. Hratchian, J. V. Ortiz, A. F. Izmaylov, J. L. Sonnenberg, D. Williams-Young, F. Ding, F. Lipparini, F. Egidi, J. Goings, B. Peng, A. Petrone, T. Henderson, D. Ranasinghe, V. G. Zakrzewski, J. Gao, N. Rega, G. Zheng, W. Liang, M. Hada, M. Ehara, K. Toyota, R. Fukuda, J. Hasegawa, M. Ishida, T. Nakajima, Y. Honda, O. Kitao, H. Nakai, T. Vreven, K. Throssell, J. A. Montgomery, Jr., J. E. Peralta, F. Ogliaro, M. Bearpark, J. J. Heyd, E. Brothers, K. N. Kudin, V. N. Staroverov, T. Keith, R. Kobayashi, J. Normand, K. Raghavachari, A. Rendell, J. C. Burant, S. S. Iyengar, J. Tomasi, M. Cossi, J. M. Millam, M. Klene, C. Adamo, R. Cammi, J. W. Ochterski, R. L. Martin, K. Morokuma, O. Farkas, J. B. Foresman, D. J. Fox, Gaussian, Inc., Wallingford CT, **2016**.
[79] M. P. Mitoraj, A. Michalak, T. Ziegler, *J. Chem. Theory Comput.* **2009**, *5*, 962.
[80] P. J. Stephens, F. J. Devlin, C. F. Chabalowski, M. J. Frisch, *J. Phys. Chem.* **1994**, *98*, 11623.
[81] S. H. Vosko, L. Wilk, M. Nusair, *Can. J. Phys.* **1980**, *58*, 1200.
[82] C. Lee, W. Yang, R. G. Parr, *Physical review. B, Condensed matter* **1988**, *37*, 785.
[83] A. D. Becke, *J. Chem. Phys.* **1993**, *98*, 5648.
[84] ADF2023, SCM, Theoretical Chemistry, Vrije Universiteit, Amsterdam, The Netherlands, http://www.scm.com.
[85] G. te Velde, F. M. Bickelhaupt, E. J. Baerends, C. Fonseca Guerra, S. J. A. van Gisbergen, J. G. Snijders, T. Ziegler, *J. Comput. Chem.* **2001**, *22*, 931.
[86] J. G. Snijders, P. Vernooijs, E. J. Baerends, *Atomic Data and Nuclear Data Tables* **1991**, *26*, 483.
[87] J. Krijn, E. J. Baerends, *Fit Functions in the HFS-Method. Internal Report (in Dutch)*, *Vrije Universiteit Amsterdam*, Amsterdam, The Netherlands, **1984**.
[88] E. van Lenthe, E. J. Baerends, J. G. Snijders, *J. Chem. Phys.* **1994**, *101*, 9783.
[89] E. van Lenthe, E. J. Baerends, J. G. Snijders, *J. Chem. Phys.* **1993**, *99*, 4597.
[90] R. E. H. Kuveke, L. Barwise, Y. van Ingen, K. Vashisth, N. Roberts, S. S. Chitnis, J. L. Dutton, C. D. Martin, R. L. Melen, *ACS Cent. Sci.* **2022**, *8*, 855.
[91] J. S. Kim, J. H. Reibenspies, M. Y. Darensbourg, *J. Am. Chem. Soc.* **1996**, *118*, 4115.
[92] N. Bandopadhyay, K. Paramanik, G. Sarkar, S. Chatterjee, S. Roy, S. J. Panda, C. S. Purohit, B. Biswas, H. S. Das, *New J. Chem.* **2023**, *47*, 9414.
[93] Y. Wang, W. Ren, J. Li, H. Wang, Y. Shi, *Org. Lett.* **2014**, *16*, 5960.
[94] T. Morofuji, Y. Matsui, M. Ohno, G. Ikarashi, N. Kano, *Chemistry (Weinheim an der Bergstrasse, Germany)* **2021**, *27*, 6713.
[95] T. Kato, S. Matsuoka, M. Suzuki, *Chem. Commun. (Camb.)* **2015**, *51*, 13906.
[96] H. van Mai, G. I. Nikonov, *Organometallics* **2016**, *35*, 943.
[97] W. Li, X.-F. Wu, *Eur. J. Org. Chem.* **2015**, *2015*, 331.
[98] M. Fagnoni, M. Mella, A. Albini, *J. Am. Chem. Soc.* **1995**, *117*, 7877.
[99] P. P. Rao, S. Nowshuddin, A. Jha, B. L. M. Rao, M. K. Divi, M. N. A. Rao, *IJC* **2022**, *61*.
[100] X. Shu, Y.-Y. Jiang, L. Kang, L. Yang, *Green Chem.* **2020**, *22*, 2734.
[101] S. Alaux, M. Kusk, E. Sagot, J. Bolte, A. A. Jensen, H. Bräuner-Osborne, T. Gefflaut, L. Bunch, *J. Med. Chem.* **2005**, *48*, 7980.

[102] I. Kisets, S. Zabelinskaya, D. Gelman, *Organometallics* **2022**, *41*, 76.
[103] J. Wang, Y. Peng, J. Xu, Q. Wu, *Org. Biomol. Chem.* **2022**, *20*, 7765.
[104] D. Arnodo, M. Ramos-Martín, L. Cicco, V. Capriati, N. Ríos-Lombardía, J. González-Sabín, A. Presa Soto, J. García-Álvarez, *Org. Biomol. Chem.* **2023**, *21*, 4414.
[105] M. Magre, E. Paffenholz, B. Maity, L. Cavallo, M. Rueping, *J. Am. Chem. Soc.* **2020**, *142*, 14286.
[106] Q. Yu, D. Zhou, Y. Liu, X. Huang, C. Song, J. Ma, J. Li, *Org. Lett.* **2023**, *25*, 47.
[107] H. Wang, Z. Wang, G. Zhao, V. Ramadoss, L. Tian, Y. Wang, *Org. Lett.* **2022**, *24*, 3668.
[108] D. Rappoport, F. Furche, *J. Chem. Phys.* **2010**, *133*, 134105.

Manuscript received: February 8, 2024
Accepted manuscript online: March 21, 2024
Version of record online: April 4, 2024